



INVESTIGATION OF CRYSTALLOGRAPHIC SLIP IN POLYCRYSTALLINE Fe₃Al USING SLIP TRACE MEASUREMENT AND MICROTTEXTURE DETERMINATION

D. RAABE, J. KEICHEL and G. GOTTSTEIN

Institut für Metallkunde und Metallphysik, Kopernikusstr. 14, RWTH Aachen, 52056 Aachen, Germany

(Received 13 November 1995; accepted 9 October 1996)

Abstract—An intermetallic Fe₇₂Al₂₈ alloy (doped with Cr, Zr, Mo, and C) with an imperfectly ordered B2 crystal structure was rolled at 830–860 K to $\epsilon = 20\%$. To investigate crystallographic slip an etching technique was developed which allowed slip traces to be determined in grain interiors rather than at the sample surface. To derive the prevalent glide systems both the slip traces and the corresponding orientations were determined in grain scale. Three types of slip systems were identified, namely $\{110\}\langle 111\rangle$, $\{112\}\langle 111\rangle$, and $\{123\}\langle 111\rangle$. However, the slip traces produced by $\{123\}\langle 111\rangle$ systems appeared wavy and were interpreted in terms of macroscopic or effective rather than crystallographic slip. The critical resolved shear stress ratio of the slip systems involved was fitted from experiment using a Relaxed Constraints Taylor model. The best correspondence between predicted and experimentally observed slip systems was attained for a critical resolved shear stress ratio of $\tau_{\{110\}}/\tau_{\{112\}} = 1.05/1.0$. © 1997 Acta Metallurgica Inc.

1. INTRODUCTION

Intermetallic Kurnakov type iron aluminides with compositions near that of Fe₃Al which are ordered to the DO₃ or imperfectly ordered to the B2 crystal structure increasingly attract attention owing to their good oxidation and sulphidation resistance, high strength at low and intermediate temperatures, low production costs, and low density [1–12]. These characteristics justified the considerable efforts made to establish Fe₃Al based alloys as a new structural material class.

However, the advantageous property profile of Fe₃Al based alloys was impaired by the lack of ductility at ambient temperature and a decrease in strength above ≈ 870 K. Since the beginning of research in this field a rapidly increasing body of literature has thus appeared, concentrating on the improvement of room temperature ductility, strength at elevated temperatures, and corrosion resistance by the control of chemical composition and microstructure.

McKamey *et al.* [7, 13] showed that an enhanced content of Cr, Si, Ta, Mo, Hf, Ti, and Nb significantly increases the yield strength of Fe₃Al at temperatures in excess of 870 K. Recent studies [10–14] confirmed that ternary additions of 2–6% Cr to DO₃ ordered iron aluminides were most effective in enhancing the room temperature ductility. Maximum values of 20% for elongation after fracture have been recently reported for Cr doped Fe₃Al by Sun *et al.* [12]. The results were interpreted in terms of the anti-phase boundary (APB) energies, change of fracture modes, and slip characteristics.

It was also shown that substitutional and interstitial additions affect the stability of the ordered phases involved. Depending on the chemical composition, the phase transformation B2 \rightarrow DO₃ ($T \approx 813$ K) can either take place directly or via decomposition into an ordered and a disordered phase, i.e. B2 \rightarrow (B2 + A2) \rightarrow (A2 + DO₃) \rightarrow DO₃ [7, 15, 16]. The formation of the DO₃ phase is typically very slow (DO₃ ordering of pure Fe₃Al at 800 K requires about 1 week) [7, 10–12]. In the presence of ternary additions like Cr, Mo, Zr, Hf, Nb, C, and B, it may even be considerably delayed [10–12]. Due to such slow transformation kinetics, recent studies have successfully focused on the partial stabilization of the imperfectly ordered B2 phase at room temperature through the employment of a so-called thermomechanical B2 treatment [10–12].

Owing to the optimization of both constitution and resulting microstructure, Fe₃Al based alloys now have improved mechanical and corrosion properties which are equivalent or even superior to those of many steels. This applies especially to their strength-to-weight ratio. Consequently, Fe₃Al based alloys are even considered nowadays as potential candidates for applications where ferritic stainless steels are in use [7].

Despite such progress in improving many technical aspects of Fe₃Al, the mechanisms that are responsible for both the strength and ductility observed are not yet sufficiently understood. This applies especially to the selection of active slip systems during large strain deformation. In fact, a quantitative analysis of how an externally imposed strain state is accomplished by crystallographic slip represents an important

approach to understanding the mechanical properties of polycrystalline Fe₃Al. Hence, this paper deals mainly with the investigation of crystallographic slip in an imperfectly B2 ordered intermetallic Fe₇₂Al₂₈ alloy, doped with Cr, Zr, Mo, and C.

2. SLIP SYSTEMS IN Fe₃Al

Most direct and indirect studies of prevalent slip systems agree that dislocation movement in Fe₃Al based alloys primarily takes place on those glide systems that are typically activated in non-ordered body centered cubic (b.c.c.) alloys. Among these, it appears that in particular $\{110\}\langle 111\rangle$ and $\{112\}\langle 111\rangle$ slip systems contribute to the accomplishment of externally imposed strains [7].

Two direct observation techniques were employed to obtain a more quantitative experimental picture of the predominant slip systems, the mechanisms of dislocation generation and movement, and of corresponding reactions in single- and polycrystalline Fe₃Al. First, slip trace investigations were conducted on the sample surface using optical microscopy. Second, direct dislocation observations were carried out employing transmission electron microscopy (TEM) [7, 14, 15, 17–21].

Thorough slip trace investigations on polished sample surfaces were conducted by Leamy *et al.* [22], Marcinkowski and co-workers [23–25], and Taoka and co-workers [26, 27] on polycrystals. These authors concentrated on the investigation of slip markings mainly with respect to their geometrical appearance (wavy or straight). However, they did not carry out complementary microtexture measurements for the determination of the respective glide systems. They reported that samples containing either 25 or 30.6 at.% Al and compressed at 300 K revealed diffuse slip markings which gradually sharpened up to a plastic strain of $\epsilon = 20\%$ (samples with 25 at.% Al) and $\epsilon = 30\%$ (samples with 30.6 at.% Al), respectively. Based on results achieved from samples with different chemical compositions and long range ordering, the two types of slip trace were interpreted in terms of deformation via ordinary (wavy) or superlattice (straight) dislocations. Although these slip trace investigations were helpful in assessing the influence of order and disorder on slip, they did not provide information about glide crystallography during polycrystal deformation in grain interiors.

Complementary slip line investigations by Schröder *et al.* [15] on Fe₇₀Al₃₀ single crystals, where the orientation of the surface plane inspected was known, revealed that both $\{110\}$ and $\{112\}$ glide planes had been activated depending on the temperature and orientation of the samples. At low temperatures up to 689 K only straight $\{110\}\langle 111\rangle$ slip traces were observed. The activation of $\{112\}\langle 111\rangle$ slip was especially noticed at temperatures above 740 K. At higher temperatures ($T \geq 870$ K) Schröder *et al.* [15] reported the occurrence of a slip plane that was

inclined by a 'few degrees away from $\{110\}$ towards $\{112\}$ '. This observation hints at the activation of $\{123\}$ slip planes. Such single crystal experiments were important for extracting information about the critical resolved shear stresses (CRSS) of $\{110\}\langle 111\rangle$ and $\{112\}\langle 111\rangle$, the slip asymmetry especially of $\{112\}\langle 111\rangle$, and the resulting orientation dependence of the activation of slip. In this context especially the anomalous course of the temperature dependence of the CRSS of Fe₃Al is of relevance [4, 28]. Single crystal experiments with various starting orientations suggested that between 270 and 550 K a negative, between 550–750 K a positive, and above 750 K again a negative temperature dependence of the CRSS occurs. Depending on the chemical composition of their alloys other authors reported somewhat different transition temperatures. Although these results provide essential insight into the deformation process of Fe₃Al, they cannot unambiguously be used for the interpretation of polycrystal deformation, where severe strain constraints already enforce multiple slip at low strains.

TEM investigations, which were carried out on deformed single- and polycrystalline material with a broad range of chemical composition and deformation temperature, showed that most Fe₃Al dislocations contained Burgers vectors parallel to $\langle 111\rangle$ [7, 14, 15, 17–21]. Furthermore, it was observed that dislocations moved on $\{110\}$ and $\{112\}$ slip planes. Similar results were reported from *in situ* TEM experiments, where dislocations were observed during rather than after straining of Fe₇₀Al₃₀ [20]. Most dislocations observed in these experiments had screw rather than edge character. This was attributed to the fact that the mobility of the edge dislocations exceeds that of the screw dislocations, which allows them to leave the TEM foils. Dislocation glide on $\{110\}$ slip planes was observed over a broad temperature interval, including regimes of both positive and negative temperature dependence of the CRSS. At the temperature of the peak strength, $T_p \approx 750$ K, slip activity was observed on $\{112\}$ slip planes. At lower temperatures ($573 \text{ K} < T < 693 \text{ K}$) $\{112\}$ planes were observed to act as cross slip or double cross slip planes.

The strength anomaly observed is commonly discussed in terms of the properties of the dislocations involved. For this purpose the results of the above cited experimental studies on prevalent slip systems has to be complemented with corresponding experimental [7] and theoretical [17–19] investigations about APB energies and dislocation core effects. In long range ordered crystals, superlattice rather than ordinary lattice dislocations are the elementary carriers of plastic flow. While in the B2 phase typically twofold-dissociated, i.e. paired $a_{B2}/2\langle 111\rangle$ dislocations prevail, in the DO₃ phase even fourfold-dissociated dislocations appear. In the latter case the $a_{B2}/2\langle 111\rangle$ pairs combine to form quadruplets, or double pairs, respectively, consisting of four partial

DO₃ superlattice dislocations with Burgers vectors $a_{DO_3}/4\langle 111 \rangle$. The motion of imperfect superlattice dislocations gives rise to the generation of APBs. In the present case the superlattice dislocations in the pairs (B2) are divided by an anti-phase boundary with a change in the nearest neighbour relation (ABP I). In the DO₃ phase the two B2 pairs are separated by a second type of anti-phase boundary with a change in the next-nearest neighbour relation (ABP II) [7, 17–19].

In this context the increase in CRSS in the temperature range 500–750 K is typically attributed to a decrease in the dislocation mobility due to a decoupling of the DO₃ superpartials. The decoupling is explained in terms of the degradation of long range order with increasing temperature. The flow stress anomaly is interpreted in terms of cross slip of superlattice dislocations from crystallographic {110} to {112} planes leaving non-mobile dislocation segments behind, which then act as barriers for further dislocation movement. Both the type of slip system and the types of superlattice dislocations involved are usually determined by composition, temperature, strain rate, and heat treatment prior to deformation [e.g. 7].

The above cited papers have pioneered the investigation of prevalent slip systems and their influence on yield strength anomaly in iron aluminides. Although they provide fundamental insight into the mechanisms of plastic flow in these alloys, there remain various open questions which could not yet be clarified by the methods employed so far.

In order to obtain information about active slip systems in polycrystalline aggregates, slip trace analysis in such samples must be carried out together with local orientation measurements. Only this combination enables one to determine the slip systems from an observed slip marking in a quantitative manner. Furthermore, geometrical aspects of slip trace investigations are important. Since plastic flow close to the sample surface is often less constrained than deformation in grain interiors, it is not clear whether slip systems that are derived from slip trace investigations on the sample surface reflect the slip behaviour in the grain interior.

Owing to such experimental shortcomings in slip trace studies, results achieved by TEM are usually considered more reliable. However, TEM studies suffer from the fact that they do not allow glide systems to be identified with sufficient statistical significance. Furthermore, TEM investigations are often carried out after deformation and on single crystals or—in case of polycrystals—without specification of the investigated grain orientation.

In this study we investigated crystallographic slip in an intermetallic Fe₇₂Al₂₈ alloy (doped with Cr, Zr, Mo, and C) with an imperfectly ordered B2 crystal structure close to the temperature of the peak strength. For this purpose, homogeneous rolling

deformation was carried out at 830–860 K. For tracking slip activity an etching technique was used, which allows slip activity to be identified in grain interiors rather than at the surface. To derive the dominating glide systems as well as the slip traces, local grain orientations were determined in the scanning electron microscope (SEM) using electron back scatter diffraction (EBSD). The CRSS ratio of the slip systems involved was fitted from experiments employing a Relaxed Constraints Taylor approach [29–32].

3. EXPERIMENTAL AND FITTING PROCEDURE

3.1. Sample preparation

According to the binary equilibrium phase diagram for Fe and Al, the investigated Fe₇₂Al₂₈ alloy has a melting temperature of 1783 K and a disordered A2 structure within the temperature range 1763–1213 K. At 1213 K a Kurnakov type phase transformation from the A2 to the imperfectly ordered B2 structure takes place. Below 813 K the ordered DO₃ (Fe₃Al) structure is stable [16]. The DO₃ unit cell consists of four interpenetrating face centered cubic (f.c.c.) sublattices, one of which is occupied entirely by aluminium atoms for the state of perfect order. For perfect B2 type long range order, two of the sublattices are occupied by aluminium atoms. Both crystal structures are related to the b.c.c. lattice. The chemical composition of the investigated alloy is given in Table 1.

The alloy was cast, thermomechanically hot rolled to a final sheet thickness of 4.86 mm, and finally annealed at 870 K. The latter two processing steps are referred to as B2 treatment [10–12]. In this state the material had a grain size of 200 μm. It contained both imperfectly ordered B2 structure and DO₃ structure. Subsequently, the samples were rolled at 830–860 K (warm rolling) to $\epsilon = 20\%$ in a strictly reversing manner, i.e. they were rotated 180° about their transverse direction between the passes. Recrystallization did not occur during warm rolling.

3.2. Slip trace investigation and microtexture determination

Deformation close to the sample surface is often less constrained than deformation in grain interiors. This applies particularly to the transverse surface of rolled specimens and typically entails sample broadening. Hence, to obtain experimental results that are not impaired by surface effects it is essential to investigate slip traces in the grain interiors rather than glide steps on the sample surface. However, the problem arising from this stipulation is that the

Table 1. Chemical composition of alloy in mass % and atomic %

	Al	Cr	Zr	Mo	C	Fe
Mass %	15.7	0.09	0.05	0.02	0.06	balance
Atomic %	27.9	0.1	0.03	0.01	0.28	balance

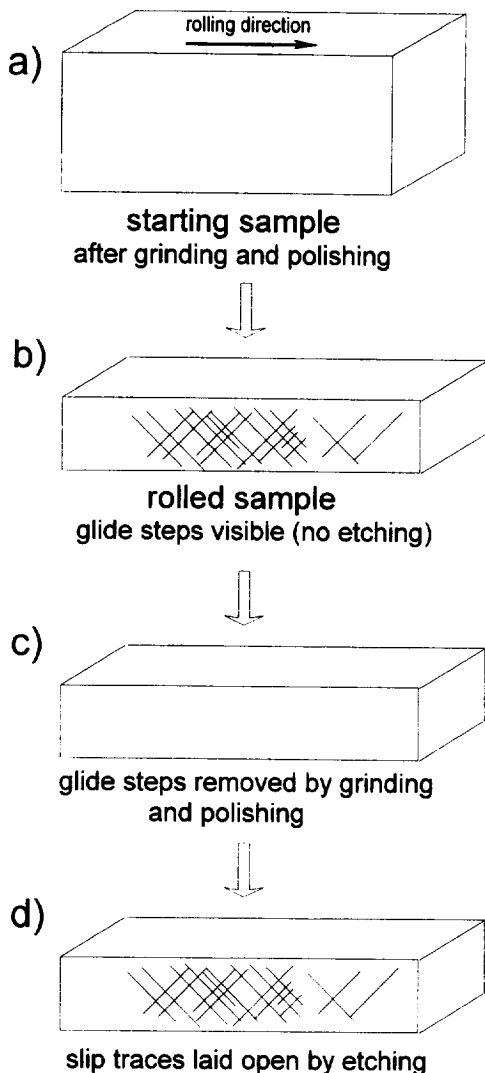


Fig. 1. Schematic explanation of the experimental procedure which was employed to prove identity of conventional surface glide steps and slip traces obtained via etching. (a) Specimen prior to rolling, (b) rolled sample with visible glide steps on its surface, (c) glide steps entirely removed by grinding and polishing, (d) etching the sample in pure HCl produced slip traces shortly before they were removed.

preparation of specimens by grinding or cutting after rolling necessarily leads to the removal of the initial glide steps on the sample surface. Nevertheless, in order to investigate slip markings in the sample interior we used a simple etching technique which allowed slip traces to be made visible after cutting and polishing, i.e. after removing the slip traces on the specimen surface. The first type of marking is hereafter referred to as (surface) glide steps and the second one as bulk slip traces.

At first it was demonstrated that the markings obtained after etching were really identical to bulk slip traces. For this purpose some specimens were cut, ground, and polished prior to deformation [Fig. 1(a)].

After rolling the surface glide steps (longitudinal sections) were investigated without any etching treatment [Fig. 1(b)]. Figures 2(a) and 3(a) clearly show that up to three different groups of such slip markings could be identified within most grains. Often some groups of glide step appeared much more distinct than others. While some slip lines were straight or only slightly curved, especially in the vicinity of grain boundaries, others appeared wavy, indicating frequent cross slip. After a thorough analysis of these surface glide steps, the samples were again ground and polished until all slip markings were entirely removed [Fig. 1(c)]. In order to demonstrate the identity of the original glide steps exposed via polishing and rolling and the bulk slip traces revealed via etching, the polished samples were then etched in pure HCl for 1–3 min. To study deformations in excess of 20%, a solution of 10 ml H_2O_2 and 1 ml HF (30 s) was used. This etching procedure indeed led again to the appearance of the slip lines which were removed shortly before and thus demonstrated their identity with the initial glide steps generated after rolling on the polished sample surface [Fig. 1(d)]. Although Figs 2(b) and 3(b) show that after etching some slip markings appeared weaker and others clearer than before, a maximum information was nevertheless extracted by using sufficiently high resolution in an SEM to allow a thorough analysis of the faint slip traces also.

The fact that slip traces can be conveniently made visible in Fe_3Al by etching offers two main experimental advantages. First, it allows crystallographic slip to be investigated not only at the sample surface but also in the sample interior. This point is of importance for a proper analysis of the results without considering surface artifacts. Second, although etching produces slip traces that are somewhat less sharp than those exposed without etching, it is more sensitive and sometimes lays open a larger number of slip markings than the conventional method. For this reason the slip traces were exclusively studied using the etching rather than the glide step technique. In order to make sure that the investigated slip traces were generated by crystallographic slip or microbands rather than by non-crystallographic shear bands, the investigations were carried out only in weakly deformed specimens ($\epsilon = 20\%$).

The textures of the specimens were examined in grain scale exploiting the anisotropy of electron back scatter diffraction in the SEM according to the method of Venables and Harland [33]. Details of the latter technique are explained elsewhere [34]. The active slip systems were derived on the basis of the experimentally observed slip traces and the corresponding local orientations. In order to obtain unambiguous solutions we skipped the analysis of special grain orientations where $\{110\}$, $\{112\}$, and $\{123\}$ planes generated similarly oriented slip traces with a mutual inclination of less than 5° .

3.3. Fitting procedure

For fitting the CRSS ratio of the slip systems involved, the experimentally observed prevalent glide systems were compared to those predicted by a Taylor Relaxed Constraints model (relaxation of ϵ_{13} and ϵ_{23} where 1 = rolling direction, 2 = transverse direction, and 3 = normal direction) [29–32]. The micrographs with the clearest slip markings were used for calibration. The ratio of the CRSS was successively changed in the Taylor simulation until a maximum agreement between the experimentally determined and the predicted slip system was achieved. In the present case the CRSS represents a somewhat artificial value. However, comprising various drags like the nucleation of superlattice dislocations, core effects, order effects, and the Peierls stress, it represents a rough measure of whether particular glide systems substantially contribute to slip or not. The increase in the CRSS with increasing

strain was assumed to be identical for all types of operative slip system. This assumption implies identical latent hardening for all slip systems and thus an isotropic growth of the yield surface. For the fitting procedure the externally imposed strain state during warm rolling was idealized as an ideal plane strain state. Such simplification seems justifiable since all investigated grains were located close to the center layer. The predications were carried out considering $\{110\}\langle 111\rangle$ and $\{112\}\langle 111\rangle$ slip systems. As will be discussed later the consideration of $\{123\}\langle 111\rangle$ slip seemed to be less meaningful due to the non-crystallographic character of the corresponding slip traces. As was shown in previous texture simulations for non-ordered b.c.c. alloys [35, 36] the asymmetry of $\{112\}\langle 111\rangle$ slip seems to be of minor importance and was hence neglected. In the Taylor model there is no need to explicitly distinguish deformation via ordinary or superlattice dislocations. This is due to the fact that in Taylor theory the glide systems are

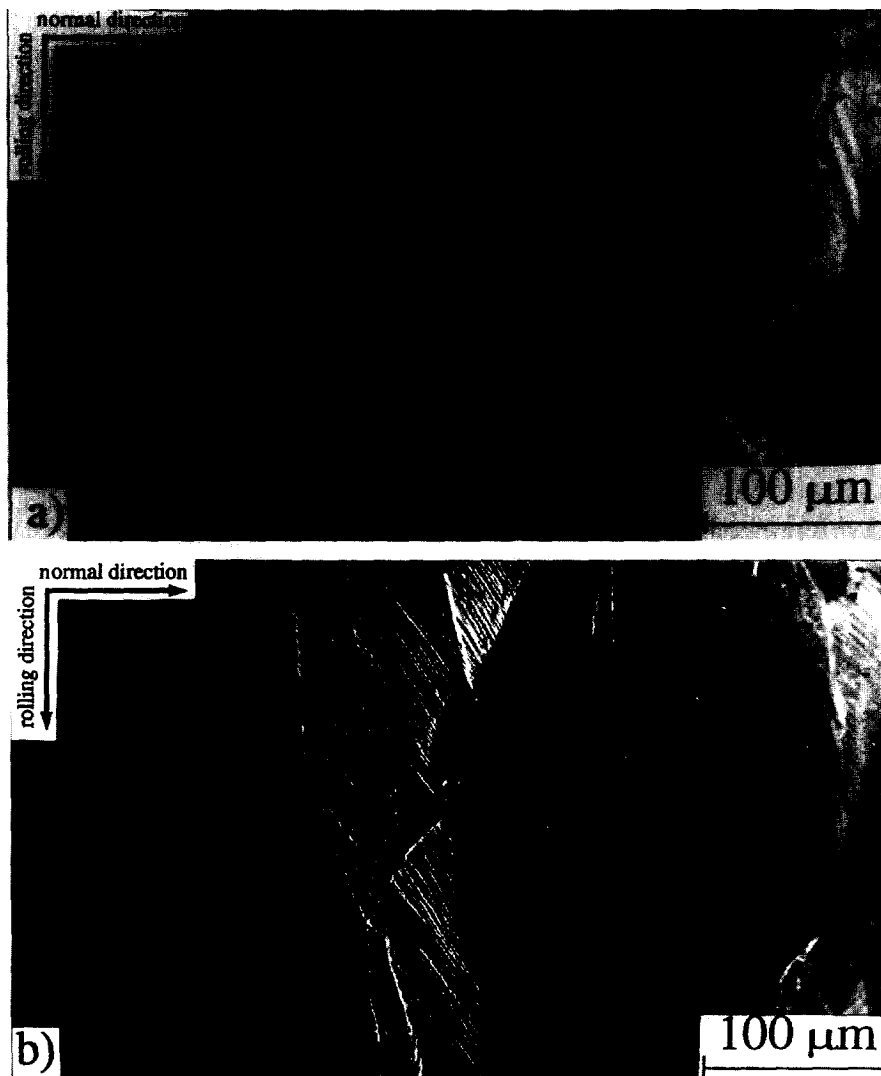


Fig. 2. Different groups of slip trace at surface of a rolled sample: (a) after rolling without etching, (b) after rolling, grinding, polishing, and etching.

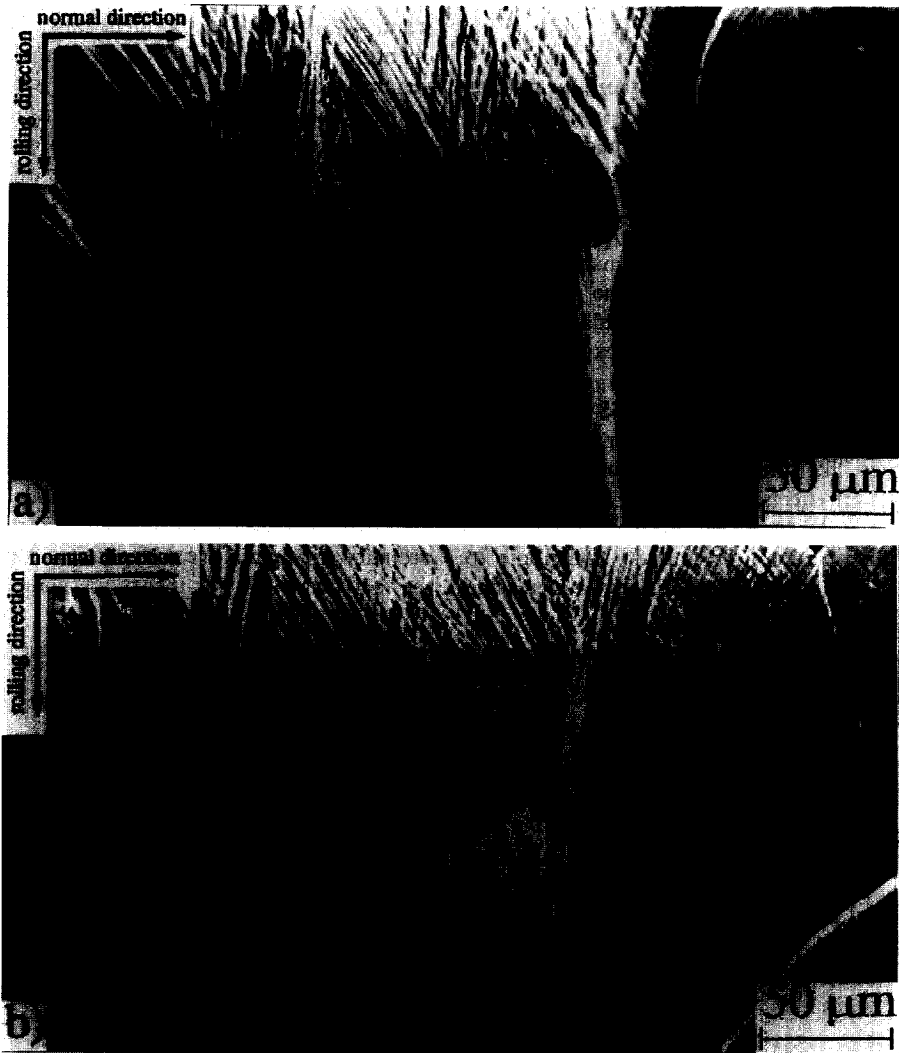


Fig. 3. Different groups of slip trace at surface of a rolled sample: (a) after rolling without etching, (b) after rolling, grinding, polishing, and etching.

reduced to their geometrical function, i.e. the entire framework of dislocation dynamics is completely neglected.

4. RESULTS

Warm rolling ($\epsilon = 20\%$) was carried out within the temperature range 830–860 K. The rolled specimens were sectioned parallel to the transverse plane, polished, and etched. Both the slip traces and the microtexture were determined in the interior of 56 different grains. In each crystal up to three groups of differently oriented slip traces were analysed. In 93 cases the observed slip markings could be unambiguously associated to $\{110\}$, $\{112\}$, or net $\{123\}$ planes.

In 45% of all investigated grains $\{110\}\langle 111 \rangle$ slip was identified. Figure 4 shows two grains in a longitudinal section. Each grain reveals two groups of straight slip trace. In both grains all traces could be attributed to $\{110\}\langle 111 \rangle$ glide systems. In many grains the occurrences of straight slip traces were due to $\{110\}$ glide. The slip trace spacing varied between

1 and 15 μm . In 46% of all examined grains $\{112\}\langle 111 \rangle$ slip was observed. In the grains depicted in Fig. 5 both $\{112\}\langle 111 \rangle$ (grain A) and $\{110\}\langle 111 \rangle$ (grain B) slip traces were identified. Both groups revealed straight slip markings and a homogeneous slip line distribution throughout the grains. The average slip trace spacing was again between 1 and 15 μm .

Of all inspected grains 77% contained net $\{123\}\langle 111 \rangle$ traces. Figure 6 shows such a grain, which is characterized by an inhomogeneous distribution of the slip traces. From this micrograph three main observations can be extracted. First, two different groups of slip markings can be identified. Position A reveals traces from intersecting $\{112\}$ and $\{123\}$ planes. At positions B and C only $\{123\}$ planes are apparent. Second, the slip markings reveal both straight and wavy shapes. Third, not only the active slip systems but also the average slip trace spacings vary. The inhomogeneity of the slip traces was also apparent in the microtexture which revealed con-

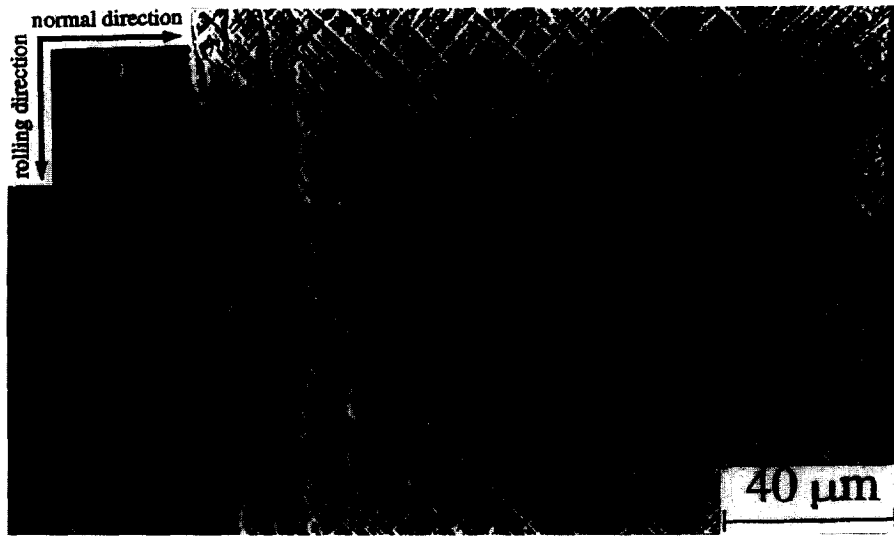


Fig. 4. Two grains in longitudinal section. Each grain contains two groups of straight slip trace.

siderable local misorientations in the grain interior. In the longitudinal section shown in Fig. 7 a large contribution of very wavy slip planes can be observed. For deriving net planes from the wavy traces their net direction rather than their local tangent direction was used. For this reason the derived planes should not be referred to as slip planes in a crystallographic sense. In most cases these wavy traces corresponded to net $\{123\}$ planes.

The experimental data are summarized in Table 2 considering $\{110\}\langle 111 \rangle$ (crystallographic), $\{112\}\langle 111 \rangle$ (crystallographic), and $\{123\}\langle 111 \rangle$ (non-crystallographic) slip systems. In the columns a '+' indicates the occurrence and a '-' the absence of the corresponding slip system. The sharpness of an etched slip trace generated by a particular slip system does not necessarily reflect its quantitative contribution to the total shear. Consequently, the analysis

is confined to the qualitative statements 'slip system is active (+)' or 'slip system is not active (-)'.

5. DISCUSSION

5.1. Orientation dependence of the experimental data

Figure 8(a) shows the symmetrized $\{100\}$ pole figure of all investigated grain orientations as determined by EBSD. The pole figure shows a weak texture with a slight pronunciation of an orientation close to the cube component having a maximum pole density of only 2.3 times random. Consequently, there is no need to take texture into account to avoid an over- or underestimation of certain slip systems.

A summary of the observed slip activity reveals that 45% of the grains show slip on $\{110\}$, 46% on $\{112\}$, and even 77% on net $\{123\}$ planes. In order to investigate whether $\{110\}$ or non- $\{110\}$ slip



Fig. 5. Two grains in longitudinal section. Grain A reveals straight $\{112\}\langle 111 \rangle$ slip traces. Grain B shows straight $\{110\}\langle 111 \rangle$ slip traces.

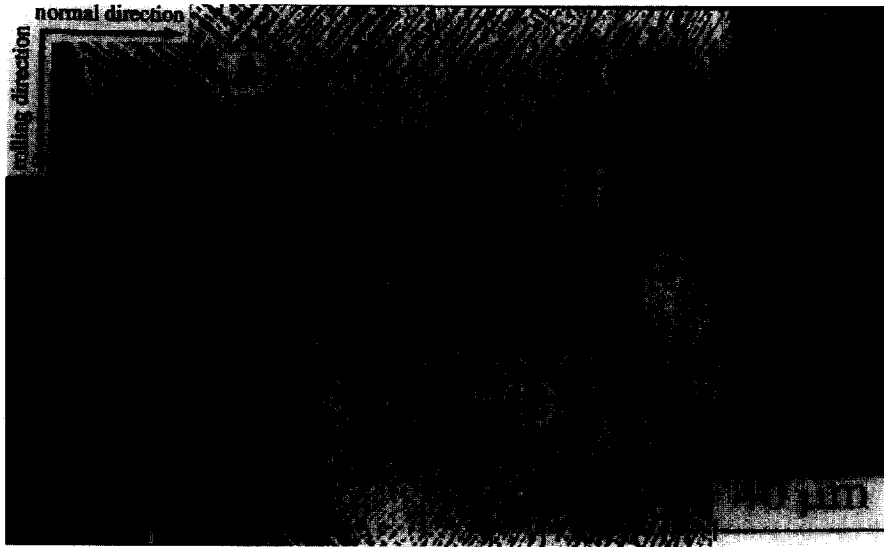


Fig. 6. Grain with a more inhomogeneous slip trace distribution. At position A interesting $\{112\}$ and $\{123\}$ slip planes were determined. At positions B and C $\{123\}$ slip planes prevail. The slip markings reveal both straight and wavy shapes.

depends on grain orientation one has to examine the orientations in which the respective type prevails. Figure 8(b) shows the symmetrized $\{100\}$ pole figure of grains in which exclusively $\{110\}$ slip planes were identified. Figures 8(a) and (b) are practically identical. That means $\{110\}$ slip was not confined to particular grain orientations. Figure 8(c) shows the symmetrized $\{100\}$ pole figure of grains in which exclusively non- $\{110\}$ slip planes were identified. Again, it does not reveal any substantial difference to the other pole figures [Fig. 8(a), (b)]. This similarity between the various pole figures shows that within the statistical limit of the present study there are no special grain orientations which promote the activation of $\{110\}$ or non- $\{110\}$ slip.

5.2. Wavy and straight slip traces

In the longitudinal sections (Figs 4–7) both straight and wavy slip traces were observed. Traces which were generated by crystallographic slip on $\{110\}$ or $\{112\}$ planes were mostly straight. In contrast, slip markings which were attributed in the analysis to net $\{123\}$ planes often had a wavy rather than a straight shape (Fig. 7). The latter result means that the observed net traces did not necessarily follow crystallographic $\{123\}$ slip planes. In a first approach, the occurrence of such non-crystallographic slip can be understood in terms of combined $\{110\}$ and $\{112\}$ slip portions in atomistic scale [37–41].



Fig. 7. Grain with very wavy slip traces. The markings correspond to net $\{123\}$ slip planes.

Table 2. Results regarding local slip activity obtained on hot rolled Fe₃Al specimens, deformed at 830–860 K to $\epsilon = 20\%$ thickness reduction

~ Crystal orientation	Experimental		
	{110}	{112}	Net {123}
{20 - 98 - 2}<-30 - 5 - 95>	+	-	-
{-98 - 7 19}<1 - 95 - 31>	+	-	-
{-4 41 - 91}<-96 - 27 - 7>	+	+	+
{94 - 14 - 31}<21 96 20>	-	+	+
{-38 32 - 87}<92 3 - 40>	-	-	+
{-94 35 6}<-10 - 10 - 99>	-	-	+
{29 - 95 10}<79 18 - 59>	-	+	-
{100-0-3}<0 100-0>	-	-	+
{80-36 48}<-24 - 93 - 29>	-	+	+
{-91 39 14}<-30 - 85 43>	-	+	+
{-25 5 97}<91 35 22>	+	-	+
{-95 - 28 15}<-9 - 21 - 97>	-	-	+
{-94 15 30}<-10 - 98 18>	-	-	+
{-96 24 - 10}<4 - 25 - 97>	+	-	+
{-94 - 24 - 25}<17 - 94 29>	+	-	-
{1 - 90 - 43}<95 14 - 27>	-	+	+
{-15 32 - 94}<97 25 - 7>	-	+	+
{-36 - 64 - 67}<28 - 77 58>	+	-	+
{19 - 98 - 4}<-64 - 10 - 76>	+	+	+
{-93 19 33}<1 - 85 52>	+	-	-
{-85 - 12 - 51}<-4 - 95 30>	+	+	+
{39 - 86 32}<-47 12 88>	+	+	+
{22 33 - 92}<97 - 5 22>	-	-	+
{-95 - 32 6}<31 - 94 - 17>	-	-	+
{-31 19 - 93}<-44 - 90 - 3>	-	+	+
{-98 6 19}<2 - 92 39>	+	-	-
{-18 - 3 - 98}<96 22 - 18>	+	-	-
{-92 24 29}<-26 16 - 95>	-	+	+
{14 13 - 98}<-31 95 9>	+	-	-
{98 - 19 7}<18 97 - 17>	-	+	-
{-87 - 39 - 31}<13 44 - 89>	+	+	+
{55 56 - 61}<70 - 71 - 2>	-	+	-
{86 35 - 39}<12 60 79>	-	+	+
{-39 2 - 92}<-0 100 2>	+	-	-
{-13 28 - 95}<97 - 16 - 17>	-	-	+
{13 91 - 39}<-95 23 21>	-	+	+
{46 - 89 2}<-33 - 15 93>	+	+	+
{-27 - 96 1}<31 - 10 - 95>	-	+	+
{28 - 87 41}<91 9 - 41>	-	+	+
{96 - 10 25}<22 - 28 - 94>	-	-	+
{-7 24 - 97}<16 - 96 - 25>	-	-	+
{-8 83 - 55}<-52 43 73>	-	-	+
{92 - 18 - 35}<25 95 17>	+	-	+
{-38 22 - 90}<84 49 - 23>	+	-	-
{-32 22 - 92}<87 47 - 18>	+	+	+
{-67 41 - 62}<-8 79 60>	-	-	+
{-37 30 - 88}<91 28 - 30>	+	+	+
{-6 97 23}<-95 2 - 32>	-	+	+
{-6 7 - 100}<-96 26 8>	-	-	+
{28 44 - 85}<-42 85 31>	+	-	+
{96 - 28 - 9}<25 93 - 27>	-	+	-
{57 - 47 - 67}<73 67 15>	+	-	+
{-46 86 - 23}<-53 - 6 85>	-	-	+
{-77 - 52 - 37}<36 - 83 42>	+	+	+
{97 - 8 - 23}<-9 77 - 63>	-	+	+
{9 99 15}<-91 2 42>	+	-	+

It is suggested that in some grains slip follows non-crystallographic planes with the maximum resolved shear stress rather than crystallographic {110} and {112} slip planes with a lower shear stress. This assumption is underlined by the fact that in grains where net {123} traces dominated, a maximum orientation factor close to 0.5 occurred on the corresponding pseudo {123}<111> system. This observation shows that in some grains the slip geometry reflects quasi-continuum rather than strictly crystallographic character.

Instead of this atomistic interpretation of non-crystallographic slip one could also think of a simple

cross slip mechanism which is not necessarily confined to the atomistic scale. In recently published *in situ* TEM studies [20] it was observed that most dislocations in Fe₃Al had screw rather than edge character. This result was in accord with previous studies [42, 43]. The lack of edge dislocations was interpreted in terms of their high mobility, which allows them to leave the TEM foils [20]. However, in the bulk sample the contribution of edge type dislocations might be larger than suggested by the TEM studies. The low mobility of the screw dislocations was attributed to the non-planar spreading of their cores [20, 37–41]. This observation

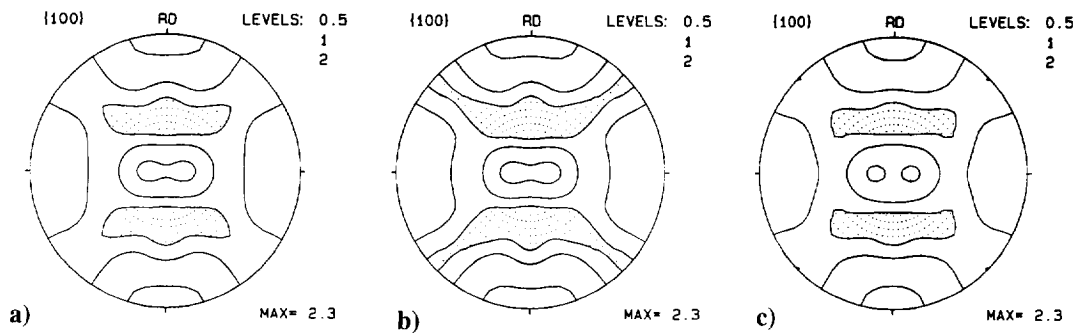


Fig. 8. Symmetrized $\{100\}$ pole figures as determined from EBSD data. (a) Texture of all investigated grains, (b) texture of grains in which $\{110\}$ slip planes were exclusively identified, (c) texture of grains in which non- $\{110\}$ slip planes were exclusively identified.

would support the assumption of frequent cross slip. In the *in situ* TEM study [20] indeed $\{112\}$ planes were frequently observed to act as cross slip or double cross slip planes for the $\{110\}$ slip systems. However, the direct observation of slip on crystal $\{123\}$ planes was not confirmed. These findings are in good accord with previous investigations on pure b.c.c. metals [37–39, 41]. On the basis of the present SEM experiments (resolution up to $20,000\times$) it cannot be decided whether non-crystallographic slip has to be interpreted in terms of alternating $\{110\}$ and $\{112\}$ slips in atomistic scale [e.g. 37–40] or in terms of simple cross slip [41]. However, one may conclude that in accord with previous TEM results on Fe_3Al [20, 42, 43], slip on crystallographic $\{123\}$ slip planes is not observed.

5.3. Activation of $\{110\}$ and $\{112\}$ slip planes

The generation and movement of superlattice dislocations in B2 and DO₃ ordered alloys is mainly determined by two properties. First by the dislocation core structure [17–19], which determines the mobility of superlattice dislocations, and second by the energy of the APB, which affects both their generation and interaction [5, 6]. The dislocation core of superpartials in the B2 lattice is similar to the core of screw dislocations in the b.c.c. lattice. Vitek [38], Wütherich [39], Duesbery [37] investigated the properties of screw and non-screw type dislocations in the b.c.c. lattice in atomistic simulations both with and without an externally imposed stress. They showed that under external stresses the non-planar core of the screw dislocations led to a net path consisting of atomistic steps on $(\bar{1}01)$, $(0\bar{1}1)$, and $(\bar{1}10)$. The properties of screw dislocations with $\langle 111 \rangle$ Burgers vector in ordered B2 alloys were correspondingly simulated by Takeuchi [40]. He observed that the cores of the partial superlattice screw dislocations were very similar to those of the ordinary b.c.c. lattice, i.e. they extended on three intersecting $\{110\}$ planes where they create stacking faults [17–19, 40]. The lowest energy arrangement of the superpartial-APB complex was a configuration where the fractional dislocations in the cores were oriented in such a way that they did

not overlap the APB. Also the three intersecting $\{110\}$ layer faults extended on the $\{112\}$ planes at their tips. In his simulations Takeuchi [40] used two different potentials to investigate the influence of both a high and a low energy APB. For the low energy case, which corresponds to the present alloy, he observed that the dislocations moved in a similar manner as in a non-ordered b.c.c. lattice.

According to Umakoshi and Yamaguchi [17–19] the energy associated with the APB on $\{110\}$ is lower than on $\{112\}$. However, they mentioned that the dislocation core is probably more extended on $\{110\}$ glide planes. Prior to its displacement the complexly dissociated dislocation core must first be converted into a planar configuration which contributes to the glide resistance. In contrast superpartials on $\{112\}$ planes create complicated multiplayer faults, which suggests that their dislocation cores are very narrow. Although they have a higher APB energy than dislocations on $\{110\}$, their core can easily transform into a glissile configuration prior to its movement. Altogether this is assumed to cause a somewhat lower glide resistance on $\{112\}$ compared to $\{110\}$ glide planes.

These structural arguments for the dominance of $\{112\}$ slip planes are supported by the fitting procedure. The best accord between the Taylor prediction and experiment is obtained when the CRSS of $\{110\}\langle 111 \rangle$ exceeds that of $\{112\}\langle 111 \rangle$ by 5%. This CRSS ratio is smaller than suggested by previous values obtained by comparing macroscopic deformation textures with Taylor type simulations [44, 45]. It suggests that the tendency for $\{112\}$ slip is not to be interpreted in terms of the APB energy but in terms of dislocation core effects. The contribution of the APB energy to the increase in energy that is required to generate new $\{112\}\langle 111 \rangle$ dislocations seems to be of minor importance.

6. CONCLUSIONS

An intermetallic $\text{Fe}_{72}\text{Al}_{28}$ alloy was warm rolled at 830–860 K to $\epsilon = 20\%$ thickness reduction. The active crystallographic slip systems were derived by

determination of slip traces in grain interiors and the corresponding grain orientations. The main conclusions are:

- In the experiments both $\{110\}\langle 111\rangle$ and $\{112\}\langle 111\rangle$ slip systems were identified with a similar slip activity. Corresponding slip traces typically had a straight shape.
- Slip on $\{123\}\langle 111\rangle$ slip systems appeared as macroscopic or effective rather than crystallographic slip. Corresponding slip traces typically had a wavy shape. It was suggested that wavy $\{123\}\langle 111\rangle$ slip can be explained by combined $\{110\}\langle 111\rangle$ and $\{112\}\langle 111\rangle$ slip.
- The critical resolved shear stresses of the involved slip systems were fitted from experiment using a Taylor Relaxed Constraints model. The best correspondence between predicted and experimentally observed slip systems was attained for a critical resolved shear stress ratio of $\tau_{\{110\}}/\tau_{\{112\}} = 1.05/1.0$.

Acknowledgements—The authors are grateful to Professor Dr Z. Sun and Professor Dr W. Mao from the Department of Materials Science and Engineering at the University of Science and Technology, Beijing, China, for providing the starting material.

REFERENCES

1. Ziegler, N., *Trans. AIME*, 1932, **100**, 267.
2. Sykes, C. and Bampfylde, J., *J. Iron Steel Inst.*, 1934, **130**, 389.
3. Davies, R. G., *J. Phys. Chem. Solids*, 1963, **24**, 985.
4. Stoloff, N. S. and Davies, R. G., *Acta metall.*, 1964, **12**, 473.
5. Leamy, H. J., Gibson, E. D. and Kayser, F. X., *Acta metall.*, 1967, **15**, 1827.
6. Leamy, H. J. and Kayser, F. X., *Phys. stat. solidi.*, 1969, **34**, 765.
7. McKamey, C. G., De Van, J. H., Tortorelli, P. F. and Sikka, V. K., *J. Mater. Res.*, 1991, **6**, 1779.
8. Golightly, F. A., Stott, F. H. and Wood, G. C., *Oxid. Metall.*, 1976, **10**, 163.
9. Tomaszewicz, P. and Wallwork, G. R., *Rev. High Temp. Mater.*, 1978, **4**, 76.
10. Chen, G., Huang, Y., Yang, W. and Sun, Z., *Proc. Conf. on Processes, Properties and Applications of Iron Aluminides*. TMS, Warrendale, USA, 1994, p. 3.
11. Sun, Z., Huang, Y., Yang, W. and Chen, G. in *High Temp. Ordered Intermetallic Alloys V*, Vol. 288, ed. I. Baker, R. Darloia, J. D. Whittenberger and M. Yoo. Mater. Res. Symp. Proc., Pittsburgh, 1993, p. 885.
12. Sun, Z., Huang, Y., Yang, W. and Chen, G., *Proc. 1994, Conf. on High Temperature Properties of Iron Based Aluminides*. TMS, San Francisco, USA, in press.
13. McKamey, C. G., Horton, J. A. and Liu, C. T., *J. Mater. Res.* 1989, **4**, 1156.
14. Morris, D. G., Dadras, M. M. and Morris, M. A., *Acta metall.*, 1993, **41**, 97.
15. Schröer, A., Hartig, C. and Mecking, H., *Z. Metallk.*, 1984, **84**, 5.
16. Masalski, T. B., *Binary Alloy Phase Diagrams*. 1986, ASM, Metals Park, Ohio.
17. Umakoshi, Y., in *Materials Science and Technology*, Vol. 6, ed. R. W. Cahn, P. Haasen and E. J. Kramer. VCH, Weinheim, 1993, p. 251.
18. Umakoshi, Y. and Yamaguchi, M., *Phil. Mag. A*, 1980, **41**, 573.
19. Umakoshi, Y. and Yamaguchi, M., *Phil. Mag. A*, 1981, **44**, 711.
20. Rösner, H., Molénat, G., Kolbe, M. and Nembach, E., *Mater. Sci. Eng. A*, 1995, **192/193**, 793.
21. Marcinkowski, M. J., in *Electron Microscopy and Strength of Crystals*. Interscience Publ. Inc., 1963, p. 333.
22. Leamy, H. J., Kayser, F. X. and Marcinkowski, M. J., *Phil. Mag.*, 1969, **20**, 763, 779.
23. Marcinkowski, M. J. and Chessin, N., *Phil. Mag.*, 1964, **10**, 837.
24. Marcinkowski, M. J. and Brown, N., *Acta metall.*, 1961, **9**, 764.
25. Marcinkowski, M. J. and Brown, N., *J. Appl. Phys.*, 1962, **33**, 537.
26. Taoka, T. and Sakata, S., *Acta metall.*, 1957, **5**, 19.
27. Taoka, T. and Honda, R., *J. Electronmicrosc. (Tokyo)*, 1957, **5**, 19.
28. Hanada, S., *Metals and Technol.*, 1984, **54**, 17.
29. van Houtte, P. and Aernoudt, E., *Z. Metallk.*, 1975, **66**, 202.
30. Honneff, H. and Mecking, H., *Proc. 5th Int. Conf. on Textures of Materials ICOTOM 5*, ed. G. Gottstein and K. Lücke. Springer Verlag, Heidelberg, 1978, p. 265.
31. van Houtte, P. in *Proc. 6th Int. Conf. on Tex. of Mat. ICOTOM 6*, ed. S. Magashima. Iron Steel Institute Jap. 1981, p. 428.
32. Kocks, U. F. and Chandra, H., *Acta metall.*, 1982, **30**, 695.
33. Venables, J. and Harland, C., *Phil. Mag.*, 1973, **27**, 1193.
34. Engler, O. and Gottstein, G., *Steel Res.*, 1992, **63**, 413.
35. Raabe, D., *Mater. Sci. Eng. A.*, 1995, **197**, 31.
36. Raabe, D., *Mater. Sci. Technol.*, 1995, **11**, 455.
37. Deusbery, M. S., in *Dislocations in Solids*. Vol. 8, ed. F. R. N. Nabarro. Elsevier Science Publishers, North Holland, 1989, p. 67.
38. Vitek, V., *Crystal Lattice Defects*, 1974, **5**, 1.
39. Wütherich, C., *Phil. Mag.*, 1977, **35**, 325.
40. Takeuchi, S., *Phil. Mag.*, 1980, **41**, 541.
41. Sesták, B. and Seeger, A., *Z. Metallk.*, 1978, **69**(4), 195; **69**(6), 355, **69**(7), 425.
42. Crawford, R. C. and Ray, I. L. F., *Phil. Mag. A.*, 1977, **35**, 549.
43. Kubin, L. P., Fourdeux, A., Guedou, J. Y. and Rieu, J., *Phil. Mag. A.*, 1982, **46**, 357.
44. Raabe, D. and Mao, W., *Phil. Mag. A.*, 1995, **71**, 805.
45. Raabe, D., *Acta metall.*, 1996, **44**, 937.